

## Yield penetration in seismically loaded anchorages: effects on member deformation capacity

S.P. Tastani\*<sup>1</sup> and S.J. Pantazopoulou<sup>2a</sup>

<sup>1</sup>Department of Civil Engineering, Democritus University of Thrace (DUTH), Vas. Sofias 12, 67100, Greece

<sup>2</sup>Department of Civil & Environmental Engineering, University of Cyprus, Nicosia 1687, Cyprus

(Received January 5, 2013, Revised July 14, 2013, Accepted July 15, 2013)

**Abstract.** Development of flexural yielding and large rotation ductilities in the plastic hinge zones of frame members is synonymous with the spread of bar reinforcement yielding into the supporting anchorage. Yield penetration where it occurs, destroys interfacial bond between bar and concrete and reduces the strain development capacity of the reinforcement. This affects the plastic rotation capacity of the member by increasing the contribution of bar pullout. A side effect is increased strains in the compression zone within the plastic hinge region, which may be critical in displacement-based detailing procedures that are linked to concrete strains (e.g. in structural walls). To quantify the effects of yield penetration from first principles, closed form solutions of the field equations of bond over the anchorage are derived, considering bond plastification, cover debonding after bar yielding and spread of inelasticity in the anchorage. Strain development capacity is shown to be a totally different entity from stress development capacity and, in the framework of performance based design, bar slip and the length of debonding are calculated as functions of the bar strain at the loaded-end, to be used in calculations of pullout rotation at monolithic member connections. Analytical results are explored parametrically to lead to design charts for practical use of the paper's findings but also to identify the implications of the phenomena studied on the detailing requirements in the plastic hinge regions of flexural members including post-earthquake retrofits.

**Keywords:** bond; slip; yield penetration; seismic assessment; drift; rotation capacity; repair

### 1. Introduction

Recent attempts to correlate analytical with experimental values of compressive strain in reinforced concrete members bent in flexure have shown that there is a consistent tendency for underestimation of the measured values. Several studies involving a variety of tests that range from walls, to bridge column tests, to FRP-jacketed R.C. flexural members, point to a higher than estimated compressive strain in the compression zone (Thermou and Pantazopoulou 2009, Thermou *et al.* 2010, Goodnight *et al.* 2012, Hannewald *et al.* 2012, Wallace *et al.* 2012). This finding is consistent with reported compression crushing failures at the base corner of structural walls in the recent earthquakes in Chile raising particular anxiety since confinement detailing in

---

\*Corresponding author, Lecturer, E-mail: [stastani@civil.duth.gr](mailto:stastani@civil.duth.gr)

<sup>a</sup> Professor, E-mail: [pantaz@ucy.ac.cy](mailto:pantaz@ucy.ac.cy)

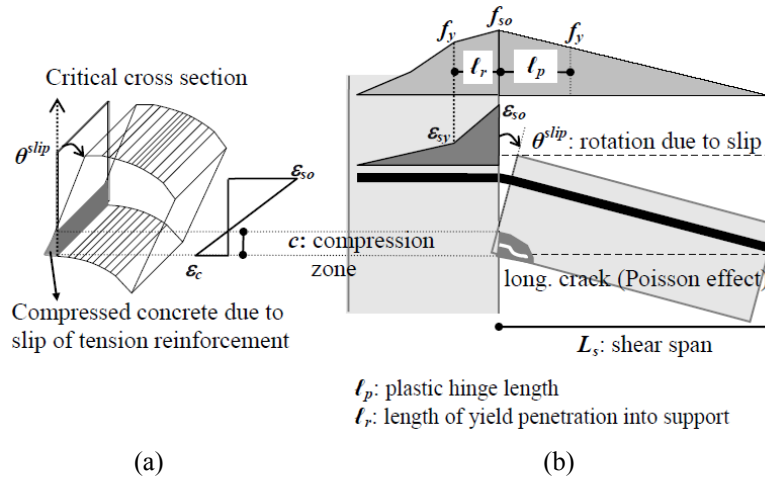


Fig. 1 The compression zone at the beam-column critical cross section cannot penetrate into the support-column to undertake to lumped rotation due to slip of tension reinforcement; instead it experiences increased contraction strain. (a) Interaction between slip and compressive strain, and (b) definition of pullout rotation

recent code revisions has been linked to the estimation of compressive strain at the extreme fiber of the wall cross section (Wallace and Moehle 2012).

Strain increase in the compression zone has also been identified theoretically and has been attributed to pullout of the tension reinforcement which causes a lumped rotation at the critical cross section near the face of the support (Syntzirma *et al.* 2010). Because the compression zone cannot penetrate into the support as would be required by the end section rotation, it is forced to undergo increased contraction strain in order to counterbalance the effects of rotation (Fig. 1). A kinematic relationship has been proposed to account for this compression strain increase, which states that the compressive strain at the extreme fiber of the cross section,  $\varepsilon_c$ , in the plastic hinge region of a flexural member, not only depends on the sectional curvature  $\phi$  and the depth of compression zone  $c$ , but also on the amount of reinforcement pullout,  $s$ , according with the following equation (Syntzirma *et al.* 2010)

$$\varepsilon_c = -\left(\phi \cdot c + \frac{s}{d-c} \cdot \frac{c}{d}\right) = -\left(\varepsilon_{so} + \frac{s}{d}\right) \cdot \frac{c}{d-c} \quad (1)$$

where,  $\varepsilon_{so}$  is the axial strain in the tension reinforcement at the critical section and  $d$  is the effective depth of the member. Eq. (1) highlights a newly identified interaction between flexural action and pullout behavior of the reinforcement: evidently, bar slip affects cross sectional equilibrium through the effect it has on  $\varepsilon_c$ . Given the cross sectional geometry and the material stress-strain laws, the resulting  $M-\phi$  relationship is no longer unique for a given axial load value (where  $M$  is the imposed moment at the critical cross section), but it depends on the details and the state of stress in the reinforcement anchorage. (For example consider a column cross section having  $d=450\text{mm}$ ,  $c=0.25d=112\text{mm}$ , and  $\varepsilon_{so}=0.005$ ; the corresponding value of  $\varepsilon_c$  is 0.0016 if slip is ignored by taking  $s=0$ , but for as small a slip value as  $s=2\text{mm}$  the corresponding concrete strain  $\varepsilon_c$  is increased to 0.003, i.e. the extreme fiber of the compression zone is at a state near crushing.)

Eq. (1) underlines the importance of dependably estimating bar slip,  $s$ , as a prerequisite to accurately evaluating the state of stress in the critical cross section of beams and columns adjacent to monolithic frame connections. Note that when the bar is strained beyond yielding, a large fraction of the slip measured in tests is owing to inelasticity spreading over the bar anchorage, a phenomenon known as yield penetration. Calculation of slip in yielding anchorages is essential for accurate interpretation of the reported failures described in the preceding. Objective of the paper is to identify the practical implications of yield penetration on rotation capacity of flexural members. This topic has particular importance in the field of seismic assessment which according with current standards, is carried out in a displacement-based framework (EC8-III 2005, ASCE/SEI 41 2007). These implications concern a number of different aspects: (a) The excessive amount of reinforcement slip from the yielded anchorage increases the flexibility of the member connection to its support, where a large fraction of the rotation is owing to reinforcement pullout from the anchorage rather than flexural curvature over the member length. (b) The kinematics of rotation due to bar pullout causes increased strains in the compression zone of the member, particularly in the plastic hinge zone adjacent to the support. Performance based detailing of certain structural members is controlled by the amount of concrete compression strains (e.g. structural walls (EC8-I 2004, ACI318 Chapter 21 2011)). In these cases, the effects of yield penetration may cancel the design objective. (c) It is shown that yield penetration may limit the strain development capacity of longitudinal reinforcement, an issue that is particularly important in existing construction where either the available anchorage is limited, or, the structural member has undergone yielding during previous seismic events thereby exhausting part of the dependable strain capacity of the anchorage of primary reinforcement.

To address these issues it is necessary to solve the equations for bond of yielding rebars so as to explore the bar strain development capacity over yielded anchorages. From a mathematical perspective, the problem of yield penetration is particularly challenging to solve since the tangent stiffness in the yield plateau is zero or lightly hardening (Soroushian *et al.* 1991, ACI 408 2012). Numerical solutions using springs along the bar to represent bond action have been attempted using a secant formulation, but this approximation has been criticized as it ignores the localization of deformation (particularly when bond springs also enter a yielding plateau or post-peak softening (Bonacci 1994, Bonacci and Ustuner 1992). An alternative approach is possible by using plasticity theory in the context of finite elements (Cox and Herrmann 1992); but in both of these numerical approaches, results are obtained at the expense of not being able to establish closed form solutions where the role of each important design parameter could be identified and illustrated. To circumvent this difficulty, in the present paper the solution for yield penetration over bar anchorages was obtained from first principles, by deriving a closed form solution of the field equations of bond using for simplicity a bilinear approximation for the post-yielding bar stress-strain law. Design charts are formulated summarizing the results of this approach, in order to relate developed bar strain of an anchorage and corresponding pullout slip with important design variables such as development length, bar size and bond strength.

## 2. Bar strain development capacity – problem definition

The case of a beam bar anchorage through a beam-column joint is probably the most severe and characteristic example of the significance of strain development capacity of the primary reinforcement anchored in the joint region and its relationship to displacement ductility. To

establish this relationship the connection is considered under moment transfer as would occur during lateral sway. Beam and column moments owing to the sway action vary linearly along the deformable member lengths with a sign reversal occurring approximately at mid-span. Inelastic strains that exceed the onset of yielding occur in the longitudinal reinforcement at the face of the support where moments attain their peak values, attenuating gradually with distance from the critical section (Fig. 1). The length over which strains exceed yielding inside the support is referred to as length of yield penetration and is denoted by  $\ell_r$  in the forthcoming derivations. The length of yield penetration on the opposite side towards the member length is referred to by convention as the plastic hinge and is denoted by  $\ell_p$  (Fig. 1). In practice, the plastic hinge length is often calculated from statics as the length of the member over which beam moments exceed the yield value

$$\ell_p = (M_u - M_y) \cdot L_s / M_u \quad (2)$$

where  $L_s$  is the member shear span,  $M_y$  and  $M_u$  are the yield and ultimate flexural strengths of the member cross section. But this alternative definition is blind to the actual state of strain in the reinforcement, where, the higher the strain at the critical section, the greater the depth to which yielding is expected to penetrate both inside the support and over the member length (Bonacci and Marquez 1994).

Consider an elastic-plastic reinforcing bar with a diameter  $D_b$ , yielding at a stress of  $f_{sy}$ . It is established in design practice to calculate the required development length of such a bar from equilibrium of forces, as  $L_b = D_b / 4 (f_{sy} / f_b^{ave})$ , which is obtained assuming a uniform bond stress  $f_b^{ave}$  over the contact length,  $L_b$ . In design calculations,  $f_b^{ave}$  is set equal to the design bond strength which depends on casting position, concrete tensile strength, bar diameter and bar rib geometry (*fib* Model Code 2010). An issue that is never explicitly addressed in this, force-based design, is, what fraction of the total available strain capacity of the bar can actually be supported if the anchorage length is set equal to the value of  $L_b$  calculated according with the stress-development needs of the bar. This concern arises from the fact that by definition, bond is zero over the yielded length of a bar; thus, when yielding spreads over a part of the available anchorage length, it effectively reduces the portion that is available for load transfer through development. It may be shown from basic stress equilibrium that there exists a critical length of  $\ell_r$ , which depends on the bar post-yielding strain at the critical section, beyond which equilibrium cannot be satisfied for the bar yield force leading to failure of the anchorage. The value of strain associated with this limit is referred to as bar strain-development capacity,  $\varepsilon_{so}^{max}$ .

In light of the fact that the nominal strain range of a bar after yielding is almost forty times greater than the strain at yielding (characteristic value:  $\varepsilon_{uk} = 0.075$  for class C, (EC2 2004)), the strain-development capacity of a yielded anchorage - which is generally smaller than  $\varepsilon_{uk}$  - may inadvertently limit the available curvature and rotation capacity of the member; note that these properties are considered till now a cornerstone of displacement-based seismic design since displacement demand may be linked directly to local plastic hinge rotation, maximum curvature and peak bar strain demand thereof, at the critical section.

Although yield penetration occurs on both sides of the critical section at the face of the support, it is interesting to note that it is not accounted for in a symmetric way in basic design. With regards to the spread of yielding inside the support, some codes assume a fixed value for  $\ell_r$  (for example,  $\ell_r$  is taken equal to  $5D_b$  in EC8-I 2004). In design, yield penetration is accounted for by simply considering this length of anchorage as inactive in force transfer. A consistent evaluation of yield

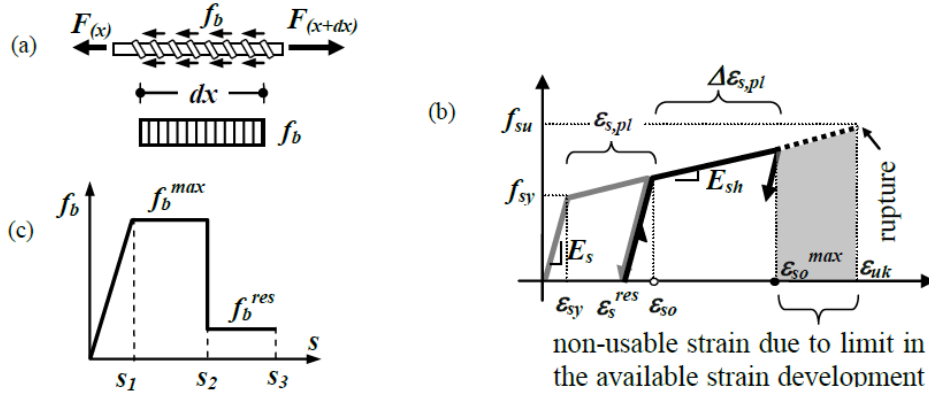


Fig. 2 (a) Force equilibrium of an elementary segment along the bar anchorage, (b) elasto-plastic stress-strain law with hardening for reinforcing steel, and (c) simplified elasto-perfectly plastic bond-slip law with a post-peak residual plateau

penetration and its effects on the strain development capacity of reinforcement may be obtained by a systematic solution of the field equations of bond for anchorages of yielded rebar. The mechanics of this problem are described in detail in the following section.

### 3. Bond assumptions for straight anchorages

Bond is defined with reference to the force equilibrium of an elementary bar segment (Fig. 2(a)). An elastic–plastic stress strain curve with hardening is used to model the behavior of steel reinforcement in tension;  $E_{sh}$  is the post-yield hardening modulus, (Fig. 2(b)). Local bond is modeled with a simplified elasto-perfectly plastic bond-slip law followed by a post-peak residual plateau (Fig. 2(c)). The initial ascending branch is modeled as a linear relationship up to the local bond strength  $f_b^{max}$  and an associated slip,  $s_1$ ; the plateau extends up to a slip value  $s_2$ , followed by a residual branch associated with pullout failure. The solution given below concerns the state of stress along a straight anchorage which is subjected to a specific strain magnitude,  $\epsilon_{so}$ , at the entrance point (i.e. at the loaded end of the anchorage, Figs. 3(a),(b)). The same solution is also valid for an anchorage with a hook, which is treated mathematically as a straight anchorage of an equivalent length  $L_{b,equiv}$  (Fig. 3(c)). This equivalent length may be calculated considering the force-anchorage capacity of an embedded hook,  $F_h$ . According to the *fib* Model Code (2010),  $F_h$  is equal to  $50f_{b,d}A_b$ , where  $f_{b,d}$  the design value of the average bond strength in the anchorage and  $A_b$  is the cross sectional area of the bar; thus the total equivalent bond force development capacity is

$$F_{equiv} = F_{straight} + F_h = \pi D_b f_{b,d} L_{b,straight} + 50 f_{b,d} \pi D_b^2 / 4 \quad (3a)$$

which corresponds to an equivalent straight development length of

$$L_{b,equiv} = L_{b,straight} + 12.5 D_b \quad (3b)$$

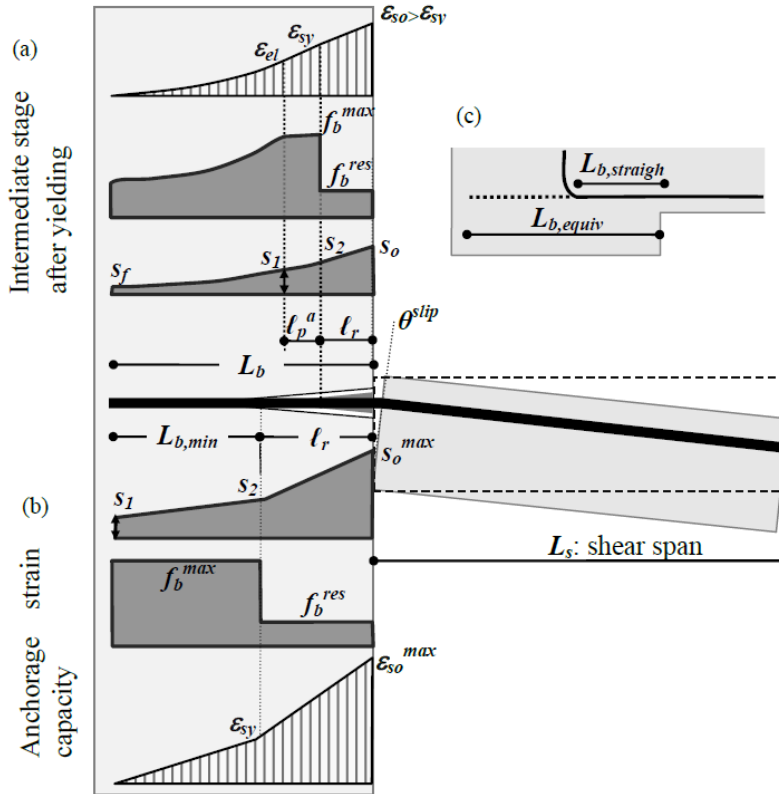


Fig. 3 The attenuations of inelastic bar strain, slip and bond stress along the anchorage are presented at (a) an intermediate strain state after yielding and (b) at the anchorage strain capacity. (c) Anchorage with a hook is treated as a straight one of equivalent length

For smooth reinforcing bars the latter equation is valid when the hook term of  $12.5D_b$  is multiplied by the ratio of design bond strength of ribbed to smooth bars ( $f_{b,rib}/f_{b,sm}$ ).

### 3.1 Governing equations of bond-slip

Consider the case where the developed strain at the critical section of the bar,  $\epsilon_{so}$ , exceeds the yield strain  $\epsilon_{sy}$  at the loaded-end of an anchorage. The general governing equations are

$$\frac{ds(x)}{dx} = -(\epsilon_s(x) - \epsilon_c(x)) \quad ; \quad \frac{df_s(x)}{dx} = -\frac{4}{D_b} f_b(x) \tag{4}$$

Solution of Eq. (4) for bar strain  $\epsilon_{so}$  greater than  $\epsilon_{sy}$  results in the Eqs. (5)-(9) listed below which define the strain, slip and bond values at characteristic points of the corresponding distributions along the embedded length (Tastani and Pantazopoulou 2012). Bond assumes values ranging from the residual resistance  $f_b^{res}$  at the loaded end, increasing to the local strength value  $f_b^{max}$  further into the anchorage, and elastic attenuation towards the tail end of the anchorage as per the distributions shown in Fig. 3(a). Three different regions are identified over the anchorage length:

(i) the segment  $\ell_r$ , adjacent to the loaded end, over which yielding has spread (strains of the segment  $\ell_r$  range from  $\varepsilon_{so}$  at the loaded end, to  $\varepsilon_{sy}$  at the end of  $\ell_r$ , Fig. 3(a)). Because the stress of a yielded bar is constant and equal to  $f_{sy}$ , it follows from Eq. (4) that local bond stress along a yielded bar is theoretically equal to zero. In the mathematical solution a slight hardening slope is used to model the plateau of the stress-strain law of the reinforcement for positive definiteness of the solution; in this segment, bond attains its residual value,  $f_b^{res}$ , thus, slip exceeds the limit value of  $s_2$  depicted in the bond stress – slip law (Fig. 2(c)).

(ii) the segment  $\ell_p^a$  further into the anchorage, over which strain attenuates from value  $\varepsilon_{sy}$  to  $\varepsilon_{el}$ , where the latter is a critical value of the bar elastic axial strain, which is associated with the onset of plastification of bond. Thus, in this segment, the bar is elastic, but the bond-slip mechanism is on its plastic plateau. Thus, the slip at the end of  $\ell_p^a$  is equal to the limit value  $s_1$  of the bond law (Figs. 2(c), 3(a)), and

(iii) the tail end of the anchorage where strain attenuates from value  $\varepsilon_{el}$  to zero (Fig. 3(a)).

Solutions for these three stages have been derived by the authors (Tastani and Pantazopoulou 2012); only expressions required to calculate the milestone points of the behavior are summarized in the following sections.

### 3.2 Definition of the minimum bonded length

Consider the instant when the bar attains its strain capacity  $\varepsilon_{so}^{max}$  at the critical section of a member's support, while at the opposite end of the anchorage the bar strain attenuates to zero. Bar slip at the bar free end approximates the characteristic value  $s_1$  of the bond – slip law (Fig. 3(b)). At imminent failure of the bar by pullout, it is assumed that yielding has penetrated deep enough into the anchorage so that the remaining bonded length  $L_{b,min}$  barely suffices to support the bar force (Fig. 3(b)). In that extreme situation of maximum attainable yield penetration, the residual bonded length must mobilize the bond strength of the material ( $f_b = f_b^{max}$ ), so that:  $L_{b,min} = D_b/4(f_{sy}/f_b^{max})$ ; thus bond stress over  $L_{b,min}$  is constant and equal to the local strength.

When considering the requirements of equilibrium over  $L_{b,min}$  for the point of imminent failure, for constant bond stress it is concluded that bar stresses attenuate linearly over the remaining bonded segment (since, according with Eq. (4),  $f_b(x)$  is proportional to  $df_b(x)/dx$ ). With the bar being elastic over this bonded part, bar strains are also linearly varying over  $L_{b,min}$ . Strains over the yielded portion,  $\ell_r$ , range from the value of  $\varepsilon_{sy}$  at the end of the  $L_{b,min}$ , to the value of  $\varepsilon_{so}^{max}$  at the critical section (Fig. 3(b)). For the assumed bond stress-slip model, bond stress is constant and equal to the residual resistance  $f_b^{res}$  over  $\ell_r$ , so a linear distribution of bar strain is assumed between  $\varepsilon_{sy}$  and  $\varepsilon_{so}^{max}$ . Clearly, higher strains than  $\varepsilon_{so}^{max}$  (the value is limited by the maximum attainable length of yield penetration) cannot be sustained in the critical section, as incipient bond failure of the bar along its anchorage will occur. For lower strain values at the critical section, ( $\varepsilon_{sy} < \varepsilon_{so} < \varepsilon_{so}^{max}$ ) the corresponding length of yield penetration  $\ell_r$  will be estimated below.

### 3.3 Calculation of milestone values of bar strain and slip along the embedded length

(i) The strain  $\varepsilon_{so}$  and slip  $s_o$  at the critical cross section (loaded-end of the anchorage where  $f_b = f_b^{res}$ ) are:

$$\varepsilon_{so} = \varepsilon_{sy} + \frac{4f_b^{res}}{D_b E_{sh}} \ell_r \Rightarrow \ell_r = (\varepsilon_{so} - \varepsilon_{sy}) \cdot \frac{D_b E_{sh}}{4f_b^{res}} \quad (5a)$$

$$s_o = s_2 + 0.5\ell_r \cdot (\varepsilon_{so} + \varepsilon_{sy}) \quad (5b)$$

where,  $\ell_r$  the yield penetration length over the anchorage, measured from the loaded end,  $s_2$  is the slip at the end of the yielded segment  $\ell_r$  (point of reference for measurements is the loaded-end, Fig. 3(a)) and  $D_b$  is the bar diameter. Through systematic calibration of the local bond - slip law it has been shown that the slip at the end of the horizontal branch,  $s_2$ , is not an intrinsic property of the bar-concrete interface but mainly depends on the anchorage length, attaining in each case its maximum value for anchorage lengths exceeding  $L_{b,min} = D_b/4 \cdot (f_{sy}/f_b^{max})$  when the anchorage attains its strain capacity value,  $\varepsilon_{so}^{max}$  (Tastani *et al.* 2012a).

(ii) With reference to Fig. 3(a) the strain  $\varepsilon_{el}$  at the end of  $\ell_p^a$  (this is the length of anchorage adjacent to  $\ell_r$ , over which bond has attained the plasticity limit  $f_b^{max}$ ), and slip  $s_2$  at the end of  $\ell_r$  and thereby at the start of  $\ell_p^a$  are

$$\varepsilon_{el} = \varepsilon_{sy} - \frac{4f_b^{max}}{D_b E_s} \ell_p^a \quad (6a)$$

$$s_2 = s_1 + 0.5\ell_p^a \cdot (\varepsilon_{sy} + \varepsilon_{el}) \quad (6b)$$

Parameter  $E_s$  is the elastic modulus of steel. Value  $s_1$  in Eq. (6b) is a characteristic property of the local bond-slip law (Fig. 2c), independent of the available anchorage length.

(iii) Over the remaining length,  $L_b - (\ell_r + \ell_p^a)$  (Fig. 3(a)) the bar is elastic, and bond stress is also on the linear ascending branch; the strain  $\varepsilon_{el}$  at the entrance point of that segment is defined through the elastic solution (Tastani and Pantazopoulou 2012) and is given by Eq. (7)

$$\varepsilon_{el} = s_1 \omega \cdot \left(1 - e^{-2\omega(L_b - \ell_r - \ell_p^a)}\right) / \left(1 + e^{-2\omega(L_b - \ell_r - \ell_p^a)}\right) ; \quad \omega = \sqrt{\frac{4f_b^{max}}{D_b E_s s_1}} \quad (7)$$

where,  $\omega$  is a measure of the elastic stiffness ( $f_b^{max}/s_1$ ) of bond as compared with that of steel,  $E_s$ . Given the developed strain value at the loaded end,  $\varepsilon_{so}$ , the system of Eqs. (5)–(7) is used to establish the unknown parameters ( $\varepsilon_{so}$ ,  $s_o$ ,  $s_2$ ,  $\varepsilon_{el}$ ,  $\ell_r$  and  $\ell_p^a$ ). Note that by combining Eqs. (6) a quadratic equation for  $\ell_p^a$  is obtained as follows

$$2f_b^{max} / (D_b E_s) \cdot (\ell_p^a)^2 - \varepsilon_{sy} \cdot \ell_p^a + (s_2 - s_1) = 0 \quad (8a)$$

The acceptable root of Eq. (8a) is the one that also satisfies the requirement of  $\ell_p^a + \ell_r \leq L_b$  and is given by

$$\ell_p^a = \frac{D_b E_s}{4f_b^{max}} \left( \varepsilon_{sy} - \sqrt{\varepsilon_{sy}^2 - 8f_b^{max} (s_2 - s_1) / (D_b E_s)} \right) \quad (8b)$$

Table 1 Definition of multiplier  $\Psi$  (where  $\Psi=L_{b,min}/D_b$ ) for several steel and concrete qualities

$f_c$ (MPa)	12	16	20	25	30	
$f_b^{max}$ (MPa)	8.7~4.3	10~5	11.2~5.6	12.5~6.3	13.7~6.8	
$f_{sy}$ (MPa)	220	7~13	6~11	5~10	5~9	4~8
	400	12~23	10~20	9~18	8~16	8~15
	500	15~29	13~25	12~23	10~20	10~19

The slip  $s_o$  at the loaded end of the anchorage is rewritten by combining Eqs. (5b) and (8a). For simplification of several terms, the definition of minimum anchorage length required for the reinforcement to develop yielding,  $L_{b,min}=(D_b/4) \cdot (E_s \varepsilon_{sy} / f_b^{max})$  is used.

$$s_o = s_1 + \left( \ell_p^a + 0.5 \ell_r - \frac{(\ell_p^a)^2}{2L_{b,min}} \right) \cdot \varepsilon_{sy} + 0.5 \ell_r \cdot \varepsilon_{so} \tag{9}$$

### 3.4 Bar strain capacity and maximum sustainable yield penetration length

The strain capacity of the bar  $\varepsilon_{so}^{max}$  and the corresponding slip designated at the loaded end,  $s_o^{max}$  are derived from Eq. (5) to Eq. (7) by substituting where  $\ell_p^a$  the value  $L_{b,min}$ . The region of maximum sustainable yield penetration is denoted as  $\ell_r=L_b-L_{b,min}$  (Fig. 3(b)).

With reference to Fig. 3(b) the ultimate slip at the bar loaded end,  $s_o^{max}$  is the result of three contributions; (i) the slip of the anchorage tail at imminent anchorage failure, which is usually omitted by several investigators in calculating the ultimate contribution of slip to chord rotation of an R.C. column. Here, this is taken equal to the slip at the end of the ascending branch of the local bond-slip law,  $s_1$ , (ii) the slip owing to integration of the linearly varying bar strains - from zero at the anchorage tail, to the yield strain  $\varepsilon_{sy}$  along the minimum bonded length  $L_{b,min}$  and (iii) the slip due to yield penetration over the debonded length  $\ell_r=(L_b-L_{b,min})$ .

#### 3.4.1 Application of the algorithm to estimation of strain development capacity

For the calculations to be easier the minimum required bonded length,  $L_{b,min}$ , is expressed as a multiple of bar diameter, as  $L_{b,min}=\Psi D_b$ . The multiplier  $\Psi$  accounts for several strength categories of steel and concrete as shown in Table 1. Note that according to the *fib* Model Code (2010) the local bond strength is taken equal to  $f_b^{max}=1.25\sim 2.5\sqrt{f_c}$ , an expression that is valid for pullout failure and for developed bar strains lower to, or equal to  $\varepsilon_{sy}$ . Note that the lower limit (i.e., 1.25) refers to favorable whereas the upper end value of 2.5 to improved bond conditions, whereas the  $\Psi$  values correspond to the straight segment of hooks and bent bars.

The strain development capacity of the reinforcement  $\varepsilon_{so}^{max}$  and the corresponding slip designated at the loaded end of the anchorage  $s_o^{max}$  are derived from Eqs. (5)-(7) by substituting where  $\ell_p^a=L_{b,min}$ . The results are given below

$$\varepsilon_{so}^{max} = \varepsilon_{sy} + 4 \cdot (L_b - L_{b,min}) \frac{f_b^{res}}{D_b E_{sh}} \Rightarrow \mu_{es} = \frac{\varepsilon_{so}^{max}}{\varepsilon_{sy}} = 1 + 4 \cdot \frac{L_b - L_{b,min}}{D_b} \cdot \frac{f_b^{res}}{E_{sh} \cdot \varepsilon_{sy}} \tag{10a}$$

$$s_o^{\max} = \underbrace{s_1}_{\text{tail}} + \underbrace{\frac{1}{2}L_{b,\min}\varepsilon_{sy}}_{\text{due to bond plastification}} + \underbrace{(L_b - L_{b,\min}) \cdot \left( \varepsilon_{sy} + 2 \cdot (L_b - L_{b,\min}) \frac{f_b^{\text{res}}}{D_b E_{sh}} \right)}_{\text{due to residual bond resistance}} \quad (10b)$$

Combining Eqs. (10a-b) the ultimate slip may be rewritten as

$$s_o^{\max} = s_1 + \frac{1}{2}L_b\varepsilon_{sy} + \frac{1}{2}(L_b - L_{b,\min}) \cdot \varepsilon_{so}^{\max} \quad (11)$$

As previously noted, the slip at the end of the horizontal branch of the local bond-slip law  $s_2$  assumes its maximum value for anchorage lengths greater than  $L_{b,\min}$  and when the anchorage strain attains the strain development capacity of the bar,  $\varepsilon_{so}^{\max}$ , thus the  $s_2$  comprises the first two parts of Eq. (10b) as

$$s_2 = s_1 + 0.5L_{b,\min}\varepsilon_{sy} \quad (12)$$

This point is also highlighted in Fig. 3(b) through the strain distribution plotted along the anchorage, where  $s_2$  is obtained from the sum of  $s_1$  and integral of bar strain over  $\ell_p^a=L_{b,\min}$ .

#### 3.4.2 Parametric Investigation of Eq. (10)

Exploring the several variables included in Eq. (10a) it is inferred that the strain capacity of the anchorage apparently depends on how deep the yield penetration may proceed, as measured by the term  $(L_b-L_{b,\min})$  and it is inversely affected by the steel hardening modulus. A stiff stress-strain response of the reinforcement after yielding reduces the strain capacity of its anchorage for a given development length  $L_b$ . On the other hand good bond conditions (for example, in the presence of the confining action exerted by stirrups, which would result to a considerable increase in residual bond strength,  $f_b^{\text{res}}$ ), can support higher tensile strains in the reinforcement. Regarding the terms of Eq. (10b) it was shown mathematically that the accumulated ultimate slip at the bar loaded end,  $s_o^{\max}$ , is the result of bar strain integration over the two segments identified in Fig. 3(b) increased by the amount of  $s_1$  of the local bond – slip law.

An important issue of the algorithm is the definition of the characteristic points in the local bond – slip law as depicted in Fig. 2(c). The values given have been obtained through consistent evaluation of a large collection of experimental data by the authors (Tastani and Pantazopoulou 2010) and are summarized for easy reference in the Appendix I.

#### 3.4.3 Development of design charts for strain development capacity

The parametric sensitivities of the strain development capacity of steel bar anchorages,  $\varepsilon_{so}^{\max}$  as well as of the associated slip at the critical section are studied in this section using the results of Eqs. (10) and (11), respectively for a 14 mm diameter bar. Results are plotted in Fig. 4 considering the strain and slip distributions depicted in Fig. 3(b). In developing this chart three alternative values were considered for the strain hardening modulus of the reinforcement,  $E_{sh}$  (5, 10 and 15% of steel's elastic modulus,  $E_s=200\text{GPa}$ ) and two different values for the local bond strength  $f_b^{\max}$  (5 and 10MPa). (Note that the average bond strength value reduced from experiments by dividing the bar force with the total nominal contact area of bar with concrete over the entire development length, is generally lower than the local bond strength value.) Other input variables required for

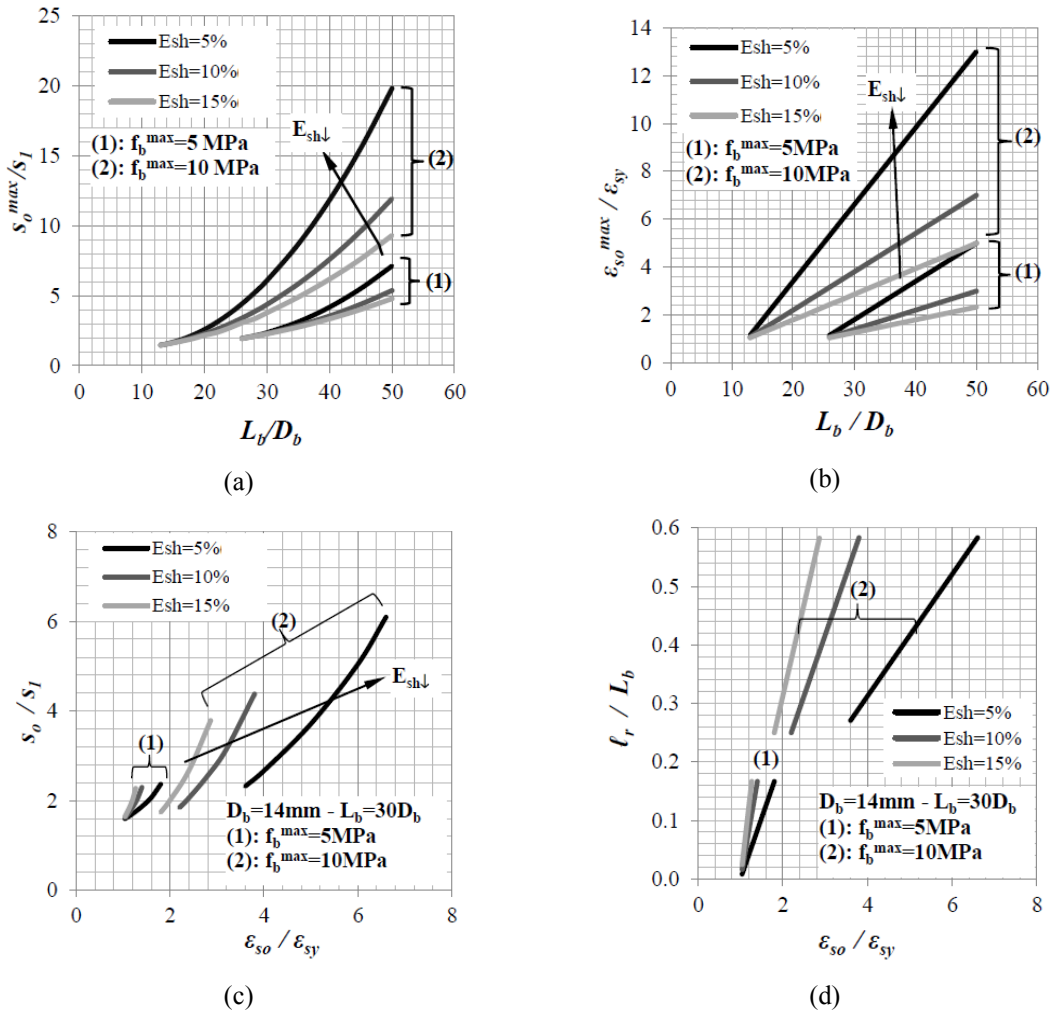


Fig. 4 Charts for the definition of (a) the slip at loaded-end of the bar anchorage and (b) the corresponding strain capacity of the anchored bar versus the embedded length for several values of steel hardening modulus ( $E_{sh}$ : 5, 10, 15%  $E_s$ ) and two values of bond strength ( $f_b^{max}=5, 10\text{ MPa}$ ). For a specific bar anchorage geometry and given the imposed strain at the loaded-end (c) the corresponding slip and (d) the debonded length are calculated

development of the graphs were,  $f_y=500\text{ MPa}$ ,  $f_b^{res}=0.2f_b^{max}$  and  $s_l=0.5\text{ mm}$ . Calculated slip values are normalized with respect to  $s_l$  (the end of the elastic range of the assumed local bond-slip law). Similarly, strains are normalized with respect to the bar's yield strain value so that the plotted value is actually the estimated strain ductility capacity of the anchorage. Graphs 4a and 4b plot the variation of these response indices against the normalized bond length, defined by  $\Psi$  or  $L_b/D_b$ . It is seen that by increasing the available anchorage length proportionately greater post-yielding strains may be sustained by the anchorage. The associated slip values increase even faster with the available development length, suggesting that: (a) total drift capacity of the concerned member increases significantly - albeit a large portion is owing to pullout- prior to failure of the

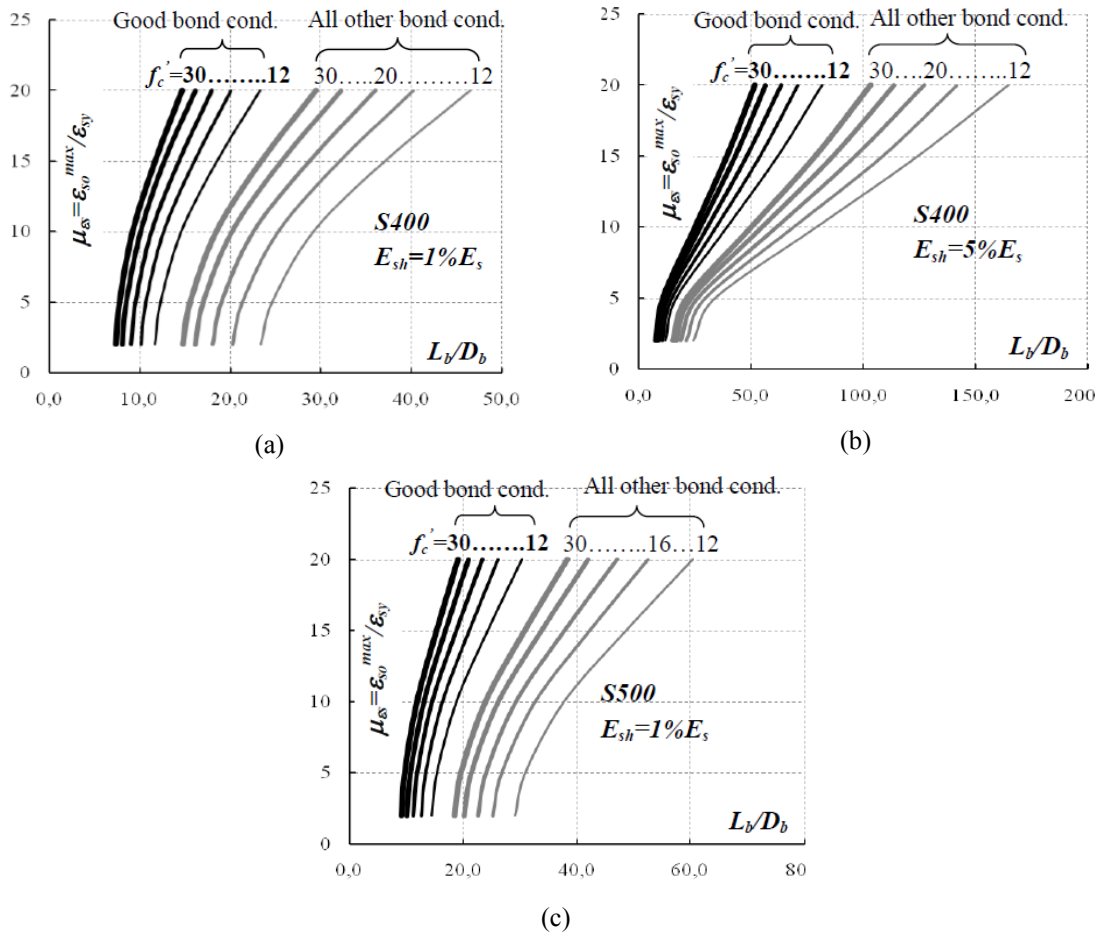


Fig. 5 Bar strain ductility capacity versus the required anchorage length for steel categories (S400 and S500), two values for hardening modulus ( $E_{sh}=1\%$  and  $5\%E_s$  for S400 and  $1\%E_s$  for S500), five concrete strengths ( $f'_c=12, 16, 20, 25, 30$ MPa) and two bond conditions

reinforcement anchorage. (b) At large drift levels a non-negligible portion of concrete strain in the compression zone of the member would be owing to slip according with Eq. (1), with implications on design and detailing requirements.

For a specific bar anchorage geometry (for example, consider the case of  $L_b/D_b=30$ ) the estimated relationship between maximum sustainable slip and bar axial strain prior to anchorage failure (where bar strain  $\epsilon_{so}$  is beyond the point of yielding:  $\epsilon_{sy} < \epsilon_{so} < \epsilon_{so}^{max}$ ) is shown in Fig. 4(c). The length of sustained yield penetration,  $\ell_r$ , normalized with respect to  $L_b$ , is plotted against bar axial strain capacity in Fig. 4(d). Note that local bond strength has a determining influence on bar axial strain capacity and yield penetration. (With reference to the example, common values in the range expected for lightly confined anchorages ( $f_b^{max}=5$ MPa, where  $f_b^{ave}=4.16$ MPa) for an anchorage length of  $30D_b$  will only enable development of a bar strain ductility less than the value of 2 and a spread of yielding over 18% of the available anchorage length. This is estimated as  $5.5D_b$ , which is consistent with the empirical postulate of EC8-I 2004.)

Fig. 4(d) underlines the fact that the available strain ductility may be much lower than the nominal value attributed to the reinforcement by either EC2 (2004) and ACI 318 (2011) based on material classification; higher strain capacities can only be relied upon if the anchorage can develop bond stresses that are significantly higher than the design values (see example with  $f_b^{max}=10\text{MPa}$  in Fig. 4(d)).

### 3.4.4 Comparison with relevant design clauses

The estimated strain ductility capacity of reinforcement  $\mu_{es} = \varepsilon_{so}^{max} / \varepsilon_{sy}$ , that can be supported by the anchorage, as calculated from Eq. (10a), is investigated below with regards to the important parameters through a sensitivity study. Fig. 5 plots term  $\mu_{es}$  against the normalized anchorage length  $\Psi = L_b / D_b$  for two steel categories (S400 and S500), five concrete types ( $f_c' = 30\text{MPa}, 25\text{MPa}, 20\text{MPa}, 16\text{MPa}$  and  $12\text{MPa}$ ), two bond conditions ( $f_b^{max}$  was taken equal to  $2.5\sqrt{f_c'}$  and  $1.25\sqrt{f_c'}$  for good and all other bond conditions respectively, values taken from Table 1) and two values for the hardening modulus of steel (1% and 5% of  $E_s (=200\text{GPa})$  for the S400 case study and only 1% $E_s$  for the case of S500). The curves in Fig. 5 are plotted with diminishing line thickness, where, the lower the concrete quality the thinner the corresponding curves. For the calculations needed to produce these plots, the residual bond strength  $f_b^{res}$  (attained after bar yielding) was estimated according with the local bond model for  $\varepsilon_{so}^{max} > \varepsilon_{sy}$ , as prescribed by the *fib* Model Code (2010). Thus,

$$f_b^{res} = f_{bm} = f_b^{max} \cdot \Omega_y; \quad \Omega_y = 1 - [0.85(1 - e^{-5\alpha^b})]; \quad \alpha = \frac{\varepsilon_{so}^{max} - \varepsilon_{sy}}{\varepsilon_{uk} - \varepsilon_{sy}}; \quad b = [2 - \frac{f_{so}^{max}}{f_{sy}}]^2 \quad (13)$$

where parameter  $\Omega_y$  accounts for the deterioration of bond as a function of the attained inelastic strain, and  $f_{so}^{max}$  the bar stress at the assumed inelastic bar strain,  $\varepsilon_{so}^{max}$ . Note that the strain at rupture of steel reinforcement was taken as  $\varepsilon_{uk}=0.08$ , whereas  $s_l$  was taken equal to 0.2mm.

The procedure followed to obtain the charts of Fig. 5 begun with the estimation of coefficients  $\alpha$  and  $b$  defined in the preceding paragraph, (from  $f_{so} = f_{sy} + E_{sh}(\varepsilon_{so}^{max} - \varepsilon_{sy})$ ), for selected reference values of the strain ductility variable, i.e., for  $\mu_{es} = 2, 5, 10, 15$  and  $20$ . Next, these are substituted in the expression for parameter  $\Omega$ , which according to *fib* Model Code (2010) multiplies the local bond strength in order to determine the residual bond strength,  $f_b^{res}$ . This is subsequently introduced in Eq. (10) and (12) and through back-calculation the required anchorage length  $L_b$  is estimated which satisfies the additional requirement to be able to develop the required ultimate strain in the anchorage,  $\varepsilon_{so}^{max}$ .

Diagrams such as those plotted in Fig. 5 can be used to assess the reinforcement strain development capacity for a known anchorage length and thus, the rotation capacity at the critical sections of frame members. Note that in a structural member, the expected bar inelastic strain capacity  $\varepsilon_{so}^{max}$  for a selected anchorage length may even be limited by other failure modes that precede anchorage failure.

The implications of limited strain development capacity of yielding reinforcement in practical seismic assessment is only considered explicitly in EC8-III (2005) which is a Code of seismic assessment of existing structures. The relevant requirements are particularly restricted to the case of straight bars lapped at the critical cross section of a frame member. According with the EC8-III (2005) requirements, the bar is able to develop its full (nominal) strain capacity  $\varepsilon_{uk}$  if the available lap length  $\ell_o$  exceeds a lower bound value, which is independent of  $\varepsilon_{uk}$

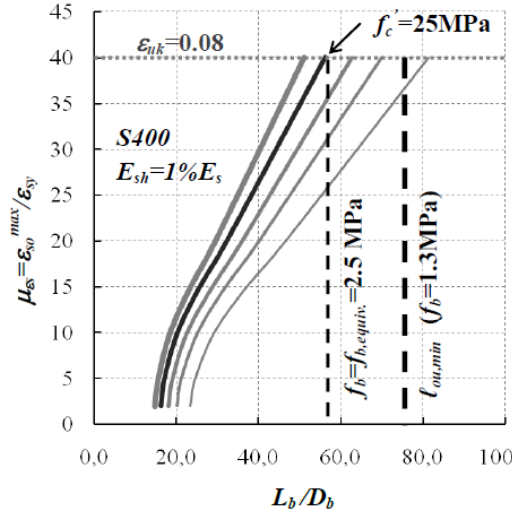


Fig. 6 Ductility  $\mu_{\varepsilon_s}$  of a straight lap splice: correlation with the EC8-III (2005)

$$\ell_{ou,min} = \frac{D_b}{1.05 + 14.5\alpha_l \rho_{sx} \frac{f_{st,y}}{f_c'}} \cdot \frac{f_{sy}}{\sqrt{f_c'}} \quad (14)$$

otherwise, the reinforcement strain capacity in the lap region is reduced by multiplying the nominal strain capacity of steel,  $\varepsilon_{uk}$ , with the ratio  $\ell_o/\ell_{ou,min}$ . Parameter  $\alpha_l$  is the confinement effectiveness for prismatic members with a rectangular cross section, equal to

$$\alpha_l = \left[ 1 - \frac{S_h}{2b_o} \right] \cdot \left[ 1 - \frac{S_h}{2h_o} \right] \cdot \frac{n_{rest}}{n_{tot}} \quad (15)$$

where  $n_{rest}$  is the number of lapped bars laterally restrained by stirrup corner or cross-tie,  $n_{tot}$  is the total number of lapped bars around the perimeter of the cross section and  $\rho_{sx} = A_{st}/(h \cdot S_h)$  the ratio of transverse steel oriented parallel to the load, and  $s_h$  the longitudinal spacing of successive stirrup layers.

When setting the minimum anchorage length,  $L_{b,min} = D_b f_{sy}/(4f_b)$  equal to  $\ell_{ou,min}$  it follows that the required average bond strength for the bar to develop its nominal strain capacity would be

$$f_b = 0.25 \cdot \left[ (1.05 + 14.5 \frac{\alpha_l \rho_{sx} f_{st,y}}{f_c'}) \sqrt{f_c'} \right] \quad (16)$$

A comparative application of the proposed model and the code expression mentioned in the preceding is presented through an example also depicted in Fig. 6 and summarized in Appendix II. From the calculations it is shown that the proposed algorithm results in a more optimistic calculation of the required bonded length than the code expression for development of the bar's nominal strain capacity.

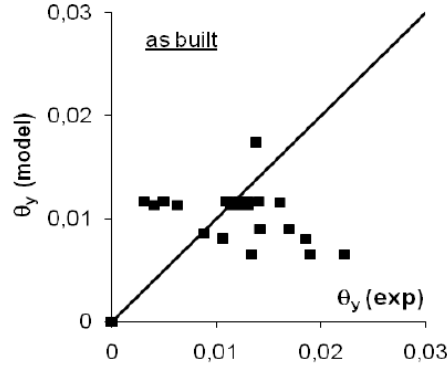


Fig. 7 Drift at yielding: correlation between analytical estimates calculated through Eq. (19) and experimental measures

#### 4. Drift components at yielding and beyond

The local strain demand that develops in the critical section of a column experiencing relative lateral drift is interpreted through the kinematics of the deformed member. Thus, if  $\theta_u$  the total chord rotation of the member, then it may be shown from concrete mechanics that the inelastic curvature at the critical section and corresponding strain of tension reinforcement are proportional to  $\theta_u$ , comprising contributions from flexural as well as pullout (slip) components

$$\theta_u = \underbrace{L_s/3 \varphi_y}_{\rho^{elastic}} + \underbrace{\ell_p (\varphi_u - \varphi_y)}_{\rho^{plastic}} + \overbrace{\left[ s_y + \left( \ell_p^a + \frac{\ell_r}{2} - \frac{(\ell_p^a)^2}{2L_{b,min}} \right) \varepsilon_{sy} + \frac{\ell_r \varepsilon_{so}}{2} \right]}^{slip} / (d - c) \Rightarrow$$

$$\theta_u = \underbrace{L_s/3 \varphi_y}_{\rho^{elastic}} + \underbrace{\ell_p (\varphi_u - \varphi_y)}_{\rho^{plastic}} + \overbrace{\frac{s_y}{d - c} + \left( \ell_p^a - \frac{(\ell_p^a)^2}{2L_{b,min}} \right) \varphi_y + \frac{\ell_r}{2} (\varphi_y + \varphi_u)}^{slip} \quad (17)$$

where,  $\ell_p$  is the plastic hinge length (in practice,  $\ell_p$  is approximated by  $0.5h$  for ribbed bars, and  $0.25h$  for smooth bars),  $\varphi_y$ ,  $\varphi_u$  are the curvatures of the critical cross section at yielding and at the inelastic state considered (Priestley *et al.* 1996, *fib* Bull. 24 2003, EC8-III 2005)

$$\varphi_y = 2.14 \varepsilon_{sy} / h \quad ; \quad \varphi_u = \varepsilon_{so} / (d - c) \quad (18)$$

where  $h$  the height of the column cross section. Similarly, the chord rotation at yielding is

$$\theta_y = \theta_y^{flex} + \theta_y^{slip} \Rightarrow \theta_y = \underbrace{L_s/3 \varphi_y}_{flexural} + \overbrace{\left[ \frac{s_y}{d - c} + \left( \ell_p^{a,elastic} - \frac{(\ell_p^{a,elastic})^2}{2L_{b,min}} \right) \varphi_y \right]}^{slip} \quad (19)$$

Parameter  $\ell_p^{a,elastic}$  is the length over the anchorage where bond has reached the state of plastification. Here, this is evaluated for the point of initiation of bar yielding at the critical section, i.e., for  $\varepsilon_{so} = \varepsilon_{sy}$ . To calculate  $\ell_p^{a,elastic}$  the following boundary conditions are introduced in Eqs. (5)-(7):  $\varepsilon_{so} = \varepsilon_{sy}$  and  $s_o = s_o^{elastic} = s_u$  whereas  $\ell_r = 0$ .

To examine the validity of Eq. (19), a database was assembled including lightly r.c. columns tested under reversed cyclic loading (Tastani *et al.* 2012b). These specimens (denoted by “as built” in Fig. 7) were subsequently repaired through FRP jacketing and retested to failure. The analytical estimation of the yield drift  $\theta_y$  (Eq. 19) as compared with the experimental estimate (point beyond which, a considerable reduction of secant flexural stiffness is observed) is shown in Fig. 7; failure was due to several reasons as reflected by the scatter, but as evidenced by Fig. 7, the rotations measured are even higher than what is estimated when accounting for slip. Obviously bond properties were even worse than assumed, and in any case values are way larger than the classical theoretical value of 0.5% for the drift at yielding, which is obtained when neglecting slip contribution.

Because the products  $s_y/(d-c) + (\ell_p^{a,elastic} - (\ell_p^{a,elastic})^2/(2L_{b,min})) \cdot \varphi_y$  and  $s_y/(d-c) + (\ell_p^a - (\ell_p^a)^2/(2L_{b,min})) \cdot \varphi_y$  (the second term corresponds to strain  $\varepsilon_{so}$ ) are of approximately equal magnitude, Eq. (17) is simplified when considering Eq. (19) as follows

$$\theta_u = \theta_y + (\ell_p + 0.5\ell_r) \cdot (\varphi_u - \varphi_y) + \ell_r \varphi_y \quad (20)$$

For the correlation of drift capacity  $\theta_u$  calculated by Eq. (20) with experimental evidence, the database presented in Tastani *et al.* (2012b) is recalled. For the definition of the analytical drift  $\theta_u$  using the database specimens (both the “as built” that were loaded up to failure and the FRP-repaired) the value of the ultimate anchorage strain  $\varepsilon_{so}^{max}$  is compared with the rupture strain of the steel  $\varepsilon_{uk}$  that is set equal to 20‰; if  $\varepsilon_{so}^{max} < \varepsilon_{uk}$  then for the calculation of  $\theta_u$  the  $\varepsilon_{so}^{max}$  is used, else the limit of  $\varepsilon_{uk}$  is used. Fig. 8 plots the analytical drift values against the experimental estimates; analyses for  $\varepsilon_{so}^{max} \leq \varepsilon_{uk}$  are plotted in Fig. 8(a) whereas Fig. 8(b) shows results from analyses using  $\varepsilon_{so}^{max}$  without any limitation in the strain capacity of the anchorage. In case of Fig. 8(a) the proposed model gives a satisfactory prediction for the “as built” specimens whereas the values for the FRP-repaired specimens are underestimated as compared with the experimental estimates. Ignoring any limitation in the strain capacity of the anchorage (i.e. using  $\varepsilon_{so}^{max}$ ) the resulting ultimate drift  $\theta_u$  of the FRP-repaired specimens presents a notable scatter. The strain hardening modulus  $E_{sh}$  is also a variable that affects the analytical results; by only increasing the hardening modulus  $E_{sh}$  from 5% to 10% $E_s$  the scatter is significantly reduced (Fig. 8(c)). Thus, the knowledge of the entire stress-strain law is very important because it impacts the accuracy of the analytical calculations of inelastic deformation capacity in r.c. members (repaired or in pristine condition).

Material strains at the critical cross section may be estimated from a first-order approximation assuming that for usual values of axial load (less than  $0.4f_c A_g$ ) the depth of compression zone  $c$  extends over 20-30% of the cross section’s effective depth  $d$ . Considering, as a simplifying approximation that the depth of compression zone does not change significantly after yielding (so that  $c$  may be taken constant), it follows from Eq. (20) that

$$\varepsilon_{s,pl} = \varepsilon_{so} - \varepsilon_{sy} = (d - c) \cdot (\varphi_u - \varphi_y) = \frac{(d - c)}{\ell_p + 0.5\ell_r} \left( \overbrace{(\theta_u - \theta_y)}^{\theta_{pl}} - \ell_r \varphi_y \right) \quad (21)$$

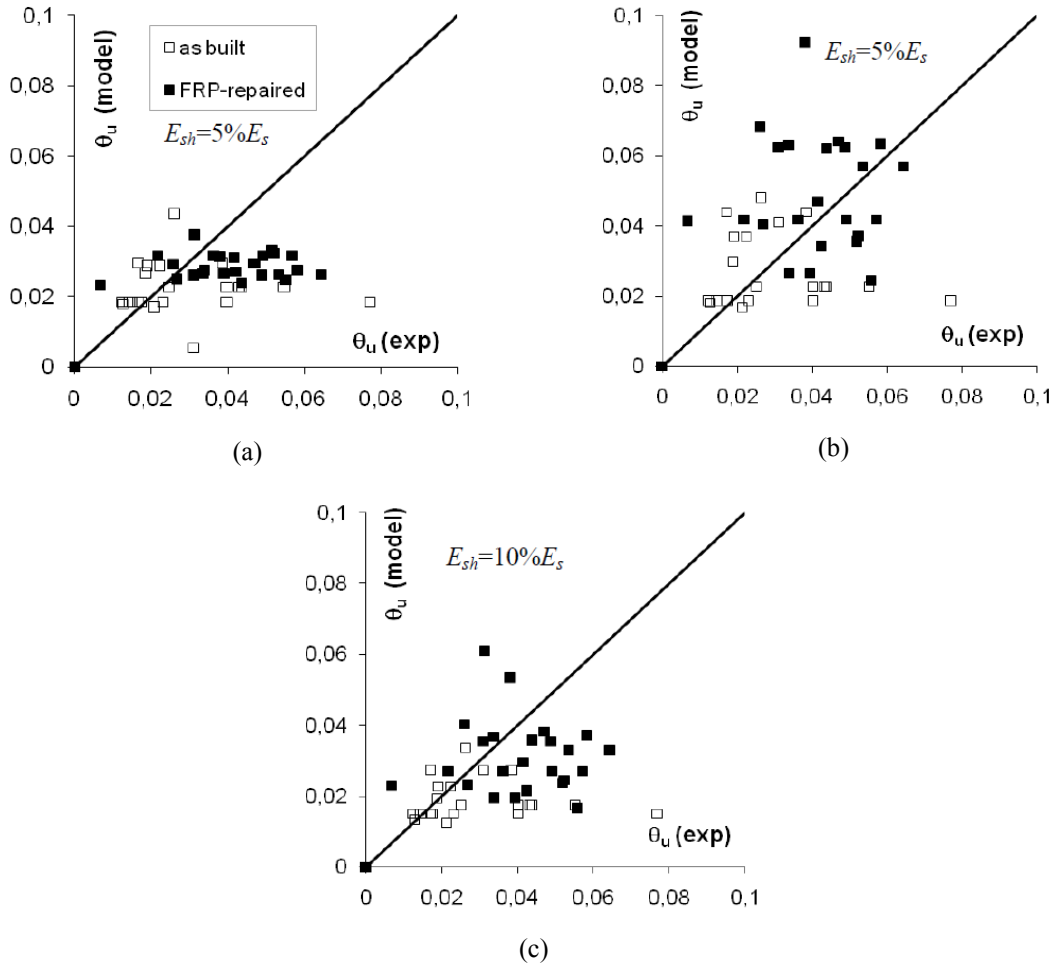


Fig. 8 Estimation of drift at ultimate,  $\theta_u$ , for both the “as built” and FRP-repaired specimens: (a) for  $\varepsilon_{so}^{max} \leq \varepsilon_r$ , (b) for  $\varepsilon_{so}^{max}$  and  $E_{sh}=5\%E_s$  and (c) for  $\varepsilon_{so}^{max}$  and  $E_{sh}=10\%E_s$

To appreciate the relative magnitude of the results a practical example is detailed below.

(Given a frame member cross section with  $h=400\text{mm}$ ,  $D_b=14\text{mm}$ ,  $L_b=30D_b$ ,  $\varepsilon_{sy}=0.0025$  ( $f_{sy}=500\text{MPa}$ ),  $f_b^{max}=10\text{MPa}$ ,  $f_b^{res}=2\text{MPa}$ ,  $s_y=0.5\text{mm}$ ,  $E_{sh}=5\%E_s$ ,  $c=0.25d$ ,  $d=370\text{mm}$ ,  $\ell_p=0.3d$ , the strain development capacity of the anchorage is obtained as follows:  $\varepsilon_{so}$  is calculated so as to satisfy both Eqs. (5)-(7) and (21) for a given drift demand. For a drift of 1.25%, where  $\theta_y=0.5\%$ , the plastic rotation demand is,  $\theta_{pl}=1.25\%-0.5\%=0.75\%$ . The value of  $\varepsilon_{so}$  is sought that satisfies Fig. 4(d) while the difference  $\varepsilon_{s,pl}=\varepsilon_{so}-\varepsilon_{sy}$  satisfies Eq. (21): it follows by trial and error that for the level of relative drift ratio considered, tension reinforcement at the critical section would sustain a bar axial strain  $\varepsilon_{so}=0.011$ , undergoing a slip value of  $s_o=1.53\text{mm}$ . In this example, the front part of the reinforcement anchorage would be debonded over a length  $\ell_r=148.8\text{mm}$ , followed by a segment  $\ell_p^a=11\text{mm}$  where bond would attain peak value corresponding to full plastification of bond.)

Eq. (21) practically states that the plastic strain,  $\varepsilon_{s,pl}$ , that occurs in the tension reinforcement is

linearly related to the inelastic drift  $\theta_{pl}$  experienced by the member. Another conclusion from the above analysis is that the larger the length of yield penetration  $\ell_r$ , the larger the fraction of the total rotation  $\theta_u$  that is owing to elastic curvature,  $\varphi_y$ , and the smaller the fraction that remains for inelastic rotation. The latter is also downsized with shorter lengths of plastic hinge in the shear span. So although the total rotation capacity may be high (i.e. in the order of 4-6%), in the presence of significant yield penetration response may be unacceptable owing to the very high compliance (flexibility) of the member to lateral displacement without toughness.

Each cycle of response to a certain drift limit pushes yield penetration deeper into the anchorage. This has significant implications on the residual strength, stiffness and deformation capacity of the member for the subsequent cycles of response. Note that if the imposed drift has exceeded even once the yielding limit, then upon unloading the tension reinforcement has residual plastic strains at the critical section (i.e.  $\varepsilon_s^{res}$  in Fig. 2(b)), their magnitude obtained from the slope of the unloading branch

$$\varepsilon_s^{res} = \left(1 - \frac{E_{sh}}{E_s}\right) \cdot \varepsilon_{s,pl} \quad (22)$$

But of far greater significance is that the residual strain capacity of the bar, which is available for future inelastic response either during subsequent cycles or in a following earthquake, is the difference of  $\Delta\varepsilon_{s,pl} = \varepsilon_{s,pl}^{max} - \varepsilon_{s,pl}$  (or better  $(\varepsilon_{so}^{max} - \varepsilon_{sy}) - \varepsilon_{s,pl}$  in case where  $\varepsilon_{so}^{max} < \varepsilon_{uk}$ , Fig. 2(b)). Therefore, in each new phase of loading (for example, after retrofit), the peak inelastic drift that may be imposed on the specimen before deterioration due to anchorage failure is only

$$\Delta\varepsilon_{s,pl} = \left(L_b - a \cdot L_{b,min}\right) \frac{4f_b^{res}}{D_b E_{sh}} - \frac{(d-c)}{\ell_p + 0.5\ell_r} (\theta_{pl} - \ell_r \varphi_y) \quad (23a)$$

In the above,  $\alpha=0.7$  if hooks are present, else  $\alpha=1$  for straight anchorages. Alternatively, the same result may be obtained by combining the Eqs. (5) and (10)

$$\Delta\varepsilon_{s,pl} = \varepsilon_{so}^{max} - \varepsilon_{so} = \left(L_b - a \cdot L_{b,min} - \ell_r\right) \frac{4f_b^{res}}{D_b E_{sh}} \quad (23b)$$

Eq. (23) identify the effects of loading history on residual deformation capacity of flexural members. A striking example is the case of FRP-jacketing of damaged columns, which became very popular on the premise of observed member behavior improvement seen in laboratory test specimens jacketed in pristine condition and subsequently tested to repeated lateral displacement reversals: In the case of columns that have experienced excessive yielding prior to jacketing, the plastic rotation capacity after jacketing is limited by the dependable residual strain range of tension reinforcement, which depends on the extent of damage that has been sustained in the anchorage – i.e. over a part of the structure that lies outside the repaired region (Thermou *et al.* 2010).

#### 4.1 Practical implications of yield penetration

##### 4.1.1 Example (a): Plastic rotation capacity of a R.C. column

To appreciate the significance of the above results consider the following numerical example on a column with a 400mm square cross section symmetrically reinforced with 5 spliced bars of

Table 2 Deformation and strength indices of the studied specimens (Syntzirma 2010, Thermou and Pantazopoulou 2009)

Name	# of layers	$\rho_{fv}$ (%)	$\theta_{y,exp}$ (%)	$\theta_{u,exp}$ (%)	$\theta_{80\%u}$ (%)	$P_y$ (kN)	$P_u$ (kN)
Ls2-b	No	---	1,10	1,76	3,50	27	34
RcLs2-b	5-C	1,10	1,74	4,72	6,93	45	45

Long. bars:  $D_b=12\text{mm}$ ,  $f_{sy}=576\text{MPa}$ ,  $f_r=670\text{MPa}$ , stirrups:  $D_{st}=6\text{mm}$ ,  $f_{st,y}=335\text{MPa}$ ,  $f_{st,r}=432\text{MPa}$ , concrete:  $f_c=20\text{MPa}$ , CFRP:  $t_f=0.11\text{mm}$ ,  $E_f=230\text{GPa}$ ,  $\varepsilon_{f,u}=0.015$ , Splice length:  $\ell_o=300\text{mm}$  ( $\ell_o/D_b=25$ ).

$D_b=16\text{mm}$  on each side of its perimeter, with  $f_{sy}=400\text{MPa}$  ( $E_s=200\text{GPa}$  and  $E_{sh}=10\text{GPa}$ ), rectangular stirrups of  $D_{b,st}=10\text{mm}$  spaced at  $S_h=100\text{mm}$  with  $f_{st,y}=220\text{MPa}$ , and a deformable length of  $3000\text{mm}$  (thus  $L_s=1500\text{mm}$ ), concrete strength  $f_c=16\text{MPa}$ , clear cover of  $c=30\text{mm}$  and anchorage length  $L_b=30D_b=480\text{mm}$ . Assumed values for the characteristic points of the bond-slip law:  $s_y=0.2\text{mm}$ , whereas for calculating  $f_b^{max}$  (see Appendix I):  $\mu=1.2$  (or  $0.6$  for the  $f_b^{res}$ ),  $\zeta=2$  and  $f_i=0.5\sqrt{f_c}$ . It is also assumed that the length of the plastic hinge  $\ell_p$  is  $0.5h$  in the shear span. The solution obtained using the proposed algorithm gives  $f_b^{max}=6.82\text{MPa}$ ,  $f_b^{res}=3.41\text{MPa}$ ,  $L_{b,min}=234.6\text{mm}$ ,  $\ell_p^{elastic}=83\text{mm}$  (at strain  $\varepsilon_{sy}=0.002$  and  $s_o^{elastic}=0.34\text{mm}$ ),  $\varphi_y=\varepsilon_{sy}/(0.7d)$  where  $d=350\text{mm}$ ,  $\varepsilon_{so}^{max}=0.023$ ,  $s_o^{max}=3.5\text{mm}$ ,  $\varphi_u^{max}=\varepsilon_{su}^{max}/(0.7d)=0.000094\text{mm}^{-1}$  and finally  $\theta_{pl}^{max}=3\%$  ( $\ell_r=245.5\text{mm}$ ,  $\theta_y=0.53\%$  - Eq. (19)),  $\theta_u^{max}=3.52\%$ . The corresponding concrete strain - neglecting the interaction between slip and flexural response - is equal to  $\varepsilon_c^{max}=\varepsilon_{so}^{max}\cdot c/(d-c)=-0.023(0.3d/0.7d)=-0.023(0.3d/0.7d)=-0.0098$ , whereas when the interaction is considered, according with Eq. (1), this value is  $-(0.023+(3.5/350))(0.3d/0.7d)=-0.014$ , i.e., a strain value 44% higher than what is obtained by the established approach used in practice.

#### 4.1.2 Example (b): Yield penetration effects on CFRP jacketing of a damaged R.C. column

Another illustration of the implications of yield penetration due to a previous loading history on the available deformation capacity of a reinforced concrete member is made with reference to an experimental example. The specimen modeled a column shear span and was tested as a cantilever having a clear height of  $900\text{mm}$ , a  $200\text{mm}$  square cross section, reinforced with 8 spliced pairs of bars placed uniformly on the perimeter of the cross section and clear cover of  $20\text{mm}$ ; rectangular stirrups were spaced at  $70\text{mm}$  o.c. One bar of each pair was anchored in the footing having a straight length of  $300\text{mm}$  and a U-shaped hook of total length  $900\text{mm}$ ; however the equivalent length was set to  $L_{b,equiv}=300+12.5D_b=450\text{mm}$ . The splice length in the column was  $\ell_o=300\text{mm}$ . The column had been originally loaded under a reversed cyclic displacement history with a combined constant axial load of  $0.08f_c A_g$  up to splitting failure along the splice length (specimen ID *Ls2\_b*, (Syntzirma *et al.* 2006)). It was subsequently repaired by cover replacement using cementitious grout and 1 layer of CFRP wrap for jacketing and retested to the same displacement history up to failure which was marked by excessive pullout of reinforcement localized at the connection between the column and the footing (specimen ID *RcLs2\_b*, outlined in Table 2 (Thermou and Pantazopoulou 2009)).

The values for the several variables needed for application of the proposed algorithm were taken as:  $f_b^{max}=6.72\text{MPa}$ ,  $f_b^{res}=3.36\text{MPa}$  (Appendix I),  $\ell_{o,min}=257\text{mm}$ , effective depth  $d=174\text{mm}$  and depth of compression zone  $c=50.5\text{mm}$  for an axial load ratio of  $0.1$ . Based on Eq. (19) the initial

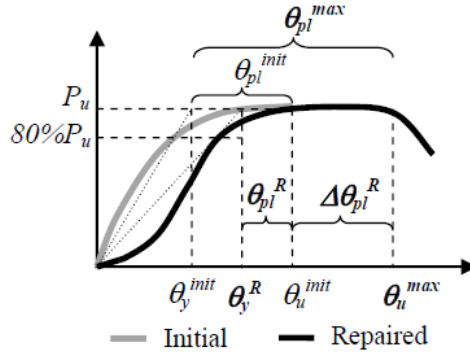


Fig. 9 Comparative representation between the initial and the confining-repaired load versus drift response of a lightly reinforced column: definition of drift indices

chord drift at yield ( $\ell_p^{elastic}=149\text{mm}$ ,  $\varphi_y=\varepsilon_{sy}/(d-c)=0.0000233\text{mm}^{-1}$ ,  $\varepsilon_{sy}=576\text{MPa}/200\text{GPa}=0.00288$ ) is  $\theta_y^{init}=1.07\%$ , a magnitude very close to the experimental measurement  $\theta_{y,exp}=1.10\%$ . Based on the drift value attained by the specimen at the termination of the initial loading phase ( $\theta_{u,exp}=1.76\%$ ) and using back-calculation (Eq. (17):  $\theta_u^{init}=\theta_{u,exp}=1.76\%$ ) the maximum curvature applied in the test was estimated:  $\varphi_u^{init}=0.00021\text{mm}^{-1}$  ( $\ell_r^{init}=26\text{mm}$ ,  $\ell_p^{init}=170\text{mm}$ ,  $\varepsilon_{so}=0.0265$ ) and the consumed plastic strain (Eq. (21)) was established  $\varepsilon_{s,pl}^{init}=0.0265-0.00288=0.0236$ , i.e., less than the dependable range of inelastic strain (Fig. 2(b)):  $\varepsilon_{s,pl}^{max}=\varepsilon_{so}^{max}-\varepsilon_{sy}=0.039$  (From Eq. (10a):  $\varepsilon_{so}^{max}=0.042$ )  $< \varepsilon_{uk}-\varepsilon_{sy}=0.08-0.00288=0.077$ .

Thus, if no other mode of failure would prevail, the splice would have a dependable strain capacity in the post-repair phase, equal to  $\Delta\varepsilon_{s,pl}=\varepsilon_{s,pl}^{max}-\varepsilon_{s,pl}^{init}=0.039-0.0236=0.0154$ . In case where no anchorage repairs are implemented to mitigate the implications of yield penetration inside the footing, (as was the case in repair of the examined specimen despite the use of cover replacement and CFRP jacketing in the plastic hinge region), the maximum drift experienced in the initial loading phase,  $\theta_{u,exp}$ , becomes the apparent chord drift at yielding in the post-repair loading phase,  $\theta_y^R$  (Fig. 9). Thus, it would be expected that  $\theta_y^R=1.76\%$ . This magnitude is very close to the experimentally measured drift at yielding of the repaired specimen  $\theta_{y,exp}=1.74\%$  (Table 2, Fig. 9) suggesting that a significant share of slip comes from the anchorage in the footing, which did not undergo any form of repair intervention in the second loading phase.

#### 4.1.3 Example (c): Increased compression strain in the compression zone of structural walls

The implications of yield penetration are most critical in design of structural walls, where a decisive criterion in detailing according with Performance Based Design principles is the magnitude of compressive strain at the extreme compression fiber of the wall cross section (Wallace and Moehle 1992, Wallace 1995). This is estimated from the ultimate drift ratio demand for the wall structure,  $\Delta_u/h_w$ , where  $h_w$  is the wall height and  $\Delta_u$  is the peak wall displacement demand at the top under the design earthquake (obtained from spectral displacement,  $S_d$ , as  $\Delta_u=S_d\cdot C_d$ ,  $S_d$  is obtained from spectral acceleration  $S_a$ , according with,  $S_d=S_aT^2/4\pi^2$ , whereas  $C_d$  is a coefficient around 1.3 required to convert spectral displacement to displacement at the top of the multistory wall structure). In design, the ultimate drift ratio demand is set equal to the local plastic

hinge rotation at the wall base,  $\theta_{pl}$ . The extreme fiber compressive strain  $\varepsilon_c$ , at the critical cross section is obtained from

$$\theta_{pl} = \frac{\Delta_u}{h_w} = \phi_u \cdot \ell_p; \quad \phi_u = \frac{\varepsilon_c}{c}; \quad \ell_p = \frac{l_w}{2}; \quad \Rightarrow \quad \varepsilon_c = 2 \cdot \frac{\Delta_u}{h_w} \cdot \frac{c}{l_w} \quad (24a)$$

where  $c$  is the depth of compression zone at the wall base and  $l_w$  is the length of the wall cross section. If the compressive strain exceeds a limiting value, typically taken as 0.003, then special transverse reinforcement is required. This is converted to a check for the depth of compression zone, against a limiting value,  $c_{limit}$  associated with attainment of the compression strain of 0.003, so that when  $c > c_{limit}$ , confined boundary elements are required in order for the wall to provide the required deformation capacity

$$c_{limit} = \frac{0.003}{2 \cdot (\Delta_u / h_w)} \cdot l_w \approx \frac{l_w}{600(\Delta_u / h_w)} \quad (24b)$$

To better match observed failures of wall tests the above was further developed to account for the influence of the wall thickness (Orakcal and Wallace 2002); however the simpler expression listed above is used for the needs of the present demonstration study, for the sake of simplicity. Consider a wall structure 10m in height, with  $l_w=2$ m, and a thickness of 200mm, reinforced in its end zones with  $D_b=20$ mm,  $f_{sy}=500$ MPa ( $\varepsilon_{sy}=0.0025$ ) longitudinal bars provided with ample anchorage inside the footing ( $L_b/D_b=50$ ). According with the above requirements, for an estimated value of plastic drift ratio,  $\theta_{pl}=0.75\%$ , the limiting compression zone depth associated with the development of a maximum compression strain of 0.003 would be for this structure, 444mm (Eq. 24b). The tension strain demand at the effective depth of the wall cross section, estimated as  $d \approx 1800$ mm, for the case considered is,  $\varepsilon_{so}=0.003 \cdot (1800-444)/444=0.0092$ , i.e., corresponding to a strain ductility of reinforcement equal to 3.7 ( $=0.0092/0.0025$ ).

Solution of the anchorage equations for this strain value at the loaded end of the typical 20mm diameter bar for  $L_b=50D_b$  leads to  $\ell_r=167.5$ mm with an associated slip value of  $s_o=1.54$ mm. For  $\theta_{pl}=0.75\%$ ,  $\ell_r=167.5$ mm and assuming a plastic hinge length  $\ell_p=0.5d=900$ mm in Eq. (21) leads to a slightly higher value for the bar strain at the critical section,  $\varepsilon_{so}=0.0122$  the difference being practically the elastic component ( $\varepsilon_{sy}=0.0025$ ) consistent with the fact that this was neglected in the design expressions used to derive  $c_{limit}$  (Eq. 24a). Using this revised value for the bar strain, and the associated slip in Eq. (1) it follows that the maximum compressive strain in the wall toe is  $\varepsilon_c = -(0.0122 + 1.54/1800) \cdot 444 / (1800 - 444) = -0.0043$ , a value that is well beyond the initial upper limit for this case, which was set equal to 0.003. Concrete cover would definitely crush at such a high strain value, leading to amplification of stresses in the confined part of the wall end; in the absence of confinement the wall cross section would experience extensive damage at this level of strain.

The increased values at the wall base thus determined underscore the significance of pullout rotation owing to penetration of yielding on the likelihood of early crushing of the compression zone if this zone is left unconfined. Note that in applying Eq. (1) to the wall cross section, it was assumed that compression zone contraction owing to pullout rotation of tension steel affects a height of the wall equal to the depth of its cross section; this assumption was extended from common frame members but may be unconservative if deeper cross sections (i.e., walls) are considered. The effect would be accentuated significantly should this strain amplification be taken

to occur over the plastic hinge. Although many other phenomena may be also responsible for the observed crushing failures in structural walls during recent earthquakes (Wallace and Moehle 2012, Wallace *et al.* 2012) such as lateral buckling due to out of plane displacements and second order effects, the significance of flexure-slip interaction described by Eq. (1) should not be overlooked in light of the significant pullout slip values due to yield-penetration, particularly if shorter anchorages/lap-splices or less favorable bond conditions prevail in field examples.

#### 4.2 Practical use of yield penetration in design

The current Codes of Seismic Assessment (EC8-III 2005, ASCE-SEI/41 2007) require that seismic demand expressed in terms of chord rotation be compared with acceptance criteria for this variable in order to establish the performance limit state for the critical structural members. Existing acceptance criteria (nominal rotational capacity) do not consider the implications of yield penetration on pullout slip nor for the limited strain capacity of reinforcement. This is corrected based on the present work as follows:

- The relationship between available anchorage length and strain development capacity plotted in Fig. 6 defines the limit in the usable strain of longitudinal reinforcement,  $\varepsilon_{so}^{max}$ . This is substituted in Eq. (18) to calculate curvatures at yield and ultimate,  $\varphi_y$  and  $\varphi_u$ . These values are substituted in Eqs. (17) and (19) to define the rotation capacity at yield and ultimate, which are proposed herein to be used as alternative acceptance criteria.

- Parameter  $\varepsilon_{so}^{max}$  is substituted in Eq. 10(b) to obtain  $s_o^{max}$ . For detailing of the compression zone of walls the compression strain demand  $\varepsilon_c$  is calculated from Eq. (1) after substitution of  $\varepsilon_{so}^{max}$  for  $\varepsilon_s$ ,  $s_o^{max}$  for  $s$ . This is compared with the concrete compression spalling strain of 0.003 to determine whether boundary confining reinforcement is required.

## 5. Conclusions

The strain development capacity of standard reinforcement anchorages was evaluated by deriving closed form solutions for the state of strain and slip along the embedment length. The analytical algorithm accounts for several design and behavioral parameters known to influence this problem, such as yield penetration in the anchorage and reduction of the effective bonded length. It is shown that the farther the spread of yielding, the smaller the amount of usable strain of the reinforcement at the critical cross section of a flexural member. Phenomena such as bond plastification and debonding of the cover after bar yielding are accounted for in order to obtain closed form solutions for the strain development capacity of yielded anchorages. Design charts that relate slip at the critical section, strain development capacity and anchorage length are developed for practical use. It is shown from first principles that the accumulated damage in the anchorage and lap splice zones of such structural elements has several implications on their seismic behavior: for one, slip of tension reinforcement causes an increase in the compression strain of flexural members in the plastic hinge region. This interaction, in the absence of confinement could cause detrimental crushing of concrete at the extreme fiber of the compression zone at lower displacement ductility levels than otherwise estimated. In retrofitted r.c. members it reduces their available post-repair ductility and inelastic deformation capacity even after jacketing. The proposed expressions are also compared with the empirical expression for strain-capacity of anchored reinforcement proposed by EC8-III (2005).

## References

- ACI 318 (2011), *Building code requirements for structural concrete (ACI 318-11) and commentary*, ACI, Farmington Hills, Michigan, USA.
- ACI 408-2R12 (2012), *Report on bond of steel reinforcing bars under cyclic loads*, ACI, Farmington Hills, Michigan, USA.
- ASCE/SEI 41 (2007), “Seismic rehabilitation of existing buildings”, American Society of Civil Engineers, Reston, VA.
- Bonacci, J. and Marquez, J. (1994), “Tests of yielding anchorages under monotonic loadings”, *J. Struct. Eng.- ASCE*, **120** (3), 987-997.
- Bonacci, J. and Ustuner, T. (1992), Discussion of “Analytical modeling of bonded bars under cyclic loads (Jan. 1991, Vol. 117, No.1)”, *J. Struct. Eng.- ASCE*, **118** (9), 2626-2628.
- Bonacci, J.F. (1994), “Bar yield penetration in monotonically loaded anchorages”, *J. Struct. Eng.- ASCE*, **120** (3), 965-986.
- Cox, J.V. and Herrmann, L. (1992), “Confinement stress dependent bond behavior, Part II: A two degree of freedom plasticity model”, *Proceedings, International Conference “Bond in Concrete”*, CEB, Riga, Latvia, Vol. 3, pp. 11-11:11-20.
- Eurocode 2 (EC2) (2004), *BS EN 1992-1-1: Design of concrete structures—general rules and rules for buildings*, European Committee for Standardization (CEN), Brussels.
- Eurocode 8 (EC8-I) (2004), *Design of structures for earthquake resistance – Part 1: General rules seismic actions and rules for buildings*, European Committee for Standardization (CEN), Brussels.
- Eurocode 8 (EC8-III) (2005), *EN1998-3-2005: Design of structures for earthquake resistance - Part 3: Assessment and retrofitting of buildings*, European Committee for Standardization (CEN), Brussels.
- Goodnight, J., Kowalsky, M., Nau, J.M. and Feng, Y.H. (2012), “Effect of load history on the behavior of circular bridge columns”, presented in the ACI341 Session: “Forming a Framework for Performance based Seismic Design of Concrete Bridges”, ACI Fall Convention, Toronto, Canada.
- Hannewald P., Beyer K. and Mihaylov B. (2012), “Performance based assessment of existing bridges with wall type piers and structural deficiencies”, presented in the ACI341 Session: “Forming a Framework for Performance based Seismic Design of Concrete Bridges”, ACI Fall Convention, Toronto, Canada.
- International Federation for Structural Concrete (*fib CEB-FIP*) (2010), *fib Model Code 2010 - Final draft*, Volume 1, *fib Bulletin No. 65*, Lausanne, Switzerland.
- International Federation for Structural Concrete (*fib*) (2003), *fib Bulletin No. 24: Seismic assessment and retrofit of reinforced concrete buildings*, State-of-art report (312 pages, ISBN 978-2-88394-064-2), Lausanne, Switzerland.
- Priestley, M.J.N., Seible, F. and Calvi, G.M. (1996), *Seismic design and retrofit of bridges*, John Wiley & Sons, Inc.
- Soroushian, P., Obasaki, K. and Marikunte, S. (1991), “Analytical modeling of bonded bars under cyclic loads”, *J. Struct. Eng.- ASCE*, **117**(1), 48-60.
- Syntzirma, D., Thermou, G., Pantazopoulou, S. and Halkitis, G. (2006), “Experimental research of R.C. elements with substandard details”, *Procs. 1<sup>st</sup> Europ. Conf. on Earthquake Engineering and Seismology*, 3–8 September, Geneva, Switzerland, pap. #: 819.
- Syntzirma, D., Pantazopoulou, S. and Aschheim, M. (2010), “Load-history effects on deformation capacity of flexural members limited by bar buckling”, *J. Struct. Eng.- ASCE*, **136**(1), 1-11.
- Tastani, S.P. and Pantazopoulou, S.J. (2007), “Detailing procedures for seismic rehabilitation of reinforced concrete members with fiber reinforced polymers”, *Eng. Struct.*, **30**(2), 450-461.
- Tastani, S.P. and Pantazopoulou, S.J. (2010), “Direct tension pullout bond test: experimental results”, *J. Struct. Eng.- ASCE*, **136**(6), 731-743.
- Tastani, S.P. and Pantazopoulou, S.J. (2013). “Reinforcement-concrete bond: state determination along the development length”, *J. Struct. Eng. – ASCE*, **139**(9), 1567-1581.

- Tastani, S.P., Thermou, G.E. and Pantazopoulou, S.J. (2012a), "Deformation analysis of reinforced concrete columns after repair with FRP jacketing", *Procs. 15th World Conference on Earthquake Engineering*, September 26-28, Lisbon, Portugal.
- Tastani, S.P., Thermou, G.E. and Pantazopoulou, S.J. (2012b), "Yield penetration in bar anchorages and the effect on rotation capacity", Vol. Compiled by the Institut für Werkstoffe im Bauwesen, Universität Stuttgart, in honor of Prof. R. Eligehausen.
- Thermou, G. and Pantazopoulou, S. (2009), "Fiber reinforced polymer retrofitting of substandard r.c. prismatic members", *J. Comp. Constr. - ASCE*, **13**(6), 535-546.
- Thermou, G., Tastani, S. and Pantazopoulou, J. (2010), "The effect of previous damage on the effectiveness of FRP-jacketing for seismic repairs of RC structural members", *Procs. 10<sup>th</sup> Int. Symposium on Fiber Reinforced Polymer Reinforcement for Reinforced Concrete Structures (SP275-54)*, October 15, Tampa, Florida, USA.
- Timosidis, D. and Pantazopoulou, S.J. (2009), "Anchorage of longitudinal column reinforcement in bridge monolithic connections", *J. Struct. Eng.- ASCE*, **135**(4), 344-355.
- Wallace, J. (1995). "Seismic design of r.c. structural walls. Part I: new code format", *J. Struct. Eng.- ASCE*, **121**(1), 75-87.
- Wallace, J.W. and Moehle, J. (2012), "Behavior and design of structural walls – lessons from recent laboratory tests and earthquakes", *Procs. International Symposium on Engineering - Lessons learned from the 2011 great east Japan earthquake*, March 1-4, Tokyo, Japan.
- Wallace, J.W., Massone, L.M., Bonelli, P., Dragovich, J., Lagos, R., Lüders, C. and Moehle, J. (2012), "Damage and implications for seismic design of RC structural wall buildings", *Earthq. Spectra*, **28**(1), 281-299.
- Wallace, J.W. and Moehle, J.P. (1992), "Ductility and detailing requirements of bearing wall buildings", *J. Struct. Eng.- ASCE*, **118**(6), 1625-1644.
- Wallace, J.W. and Orakcal K. (2002), "ACI 318-99 provisions for seismic design of structural walls", *ACI Struct. J.*, **99**(4), 499-508.

## Appendix I: Bond – slip relationship

The ascending branch of the local bond – slip law is linearly elastic up to attainment of the bond strength  $f_b^{max}$  associated with a slip  $s_l=0.2-0.3\text{mm}$  for bars with a normal rib area in the order of  $f_R=0.07$ . After this point bond enters a state of plastification where local bond-stress is constant and equal to the strength,  $f_b^{max}$ , up to a slip magnitude  $s_2$  (Fig. 2(c)). The slip  $s_2$  is not an intrinsic property of the bar-concrete interface as it mainly depends on the anchorage length. It takes on its maximum value for anchorage lengths greater than the minimum length  $L_{b,min}$  and when the strain attains the capacity  $\varepsilon_{so}^{max}$ . The local bond strength  $f_b^{max}$  of anchorages confined with transverse reinforcement (stirrups or FRP jackets) is defined as (Tastani and Pantazopoulou 2007)

$$f_b^{max} = \frac{2\mu}{\pi} \cdot \left( \zeta \frac{C}{D_b} f_t' + 0.33 \frac{A_{st} f_{st,y}}{D_b N_b S_h} + \frac{2t_j E_f \varepsilon_{f,eff}}{D_b N_b} \right) \quad (A1)$$

where  $\mu$  is the coefficient of friction along the splitting plane (0.9-1.2 for ribbed, and 0.3 for smooth reinforcement),  $\zeta$  accounts for the tensile behavior of the concrete cover (1 for fully elastic and 2 for fully plastic),  $C$  is the clear cover thickness,  $f_t'$  is concrete's tensile strength ( $0.35 \sim 0.5 \sqrt{f_c}$ ),  $N_b$  is the number of tension bars restrained by the stirrup legs included in  $A_{st}$  ( $A_{st}$  is the cross sectional area of stirrups crossing the splitting plane),  $S_h$  is the stirrup spacing,  $f_{st,y}$  the stirrup yield stress. The third term in Eq. (A1) is omitted in rehabilitated cases in the absence of confining FRP jackets over laps ( $t_j$ ,  $E_f$  and  $\varepsilon_{f,eff}$  are the FRP jacket thickness, the material modulus of elasticity and its effective strain as a mechanism of confinement for laps,  $\varepsilon_{f,eff}$  in the range of 0.0015~0.002). In laps that have been split lengthwise prior to jacketing, the development capacity after the addition of the jacket is only marginally improved unless cover replacement has preceded the jacketing. Similarly, in damaged anchorages where spread of yielding has penetrated into the anchorage, bond is destroyed except for the clamping force exerted by transverse reinforcement at the discrete locations of contact between stirrups and the main bars (Timosidis and Pantazopoulou 2009). This type of damage needs to be mitigated (e.g. by epoxy injections) in order to recover the original strength of the interface and member stiffness. Thus, the possibility of prior longitudinal cracking in the cover eliminates the first term in Eq. (A1), with commensurate implications on the strain development capacity of the anchorage.

The residual bond strength  $f_b^{res}$  developed over the yield penetration length of the anchorage may be calculated using Eq. (A1) by assuming that the frictional coefficient  $\mu$  reduces to a residual value in the order of  $\mu^{res}=0.4 \sim 0.6$  as long as the ultimate slip  $s_o$  of the critical section does not exceed the rib spacing  $s_3$  (see also Fig. 2(c)); beyond this threshold  $\mu^{res}$  is taken equal to zero.

## Appendix II – Example: confined anchorage requirement

**Example:** According with EC 8-III (2005), a non-confined (no stirrups) lap-spliced bar with  $f_{sy}=400\text{MPa}$  ( $E_s=200\text{GPa}$  and  $E_{sh}=1\%E_s=2\text{GPa}$ ) and concrete strength  $f_c=25\text{MPa}$  requires an average bond strength equal to  $f_b=0.25 \cdot [(1.05+0) \sqrt{25}]=1.3\text{MPa}$  in order for the bars to be able to develop their nominal strain capacity of  $\varepsilon_{uk}=0.08$  (i.e., a strain ductility  $\mu_{\varepsilon}=\varepsilon_{so}^{max}/\varepsilon_{sy}$  of 40) over a length  $\ell_{ou,min}=D_b \cdot 400/(4 \cdot 1.3) \approx 77D_b$  (thicker dashed line, Fig. 6). For the problem of an anchorage of equal length, using the algorithm proposed in this paper, for the bars to be able to sustain yielding to the same nominal strain ductility,  $\mu_{\varepsilon}=40$ , it follows that the required normalized lapped (or embedded) length is,  $L_b/D_b=56$  (mid-thick dashed line, Fig. 6). In this case, at the onset of failure, bond would reach the local bond strength,  $f_b^{max}=6.25\text{MPa}$  for a length of  $\ell_p^a/D_b=L_{b,min}/D_b=16$ , (for concrete  $f_c=25\text{MPa}$ , black curve in Fig. 6, see also Table 1) along the last part of the anchorage whereas over the remaining yielded length,  $\ell_r=(L_b-L_{b,min})=40D_b$ , bond stress would be equal to the residual bond strength,  $f_b^{res} \approx 1\text{MPa}$ . The corresponding average bond strength for this calculation is  $f_b^{ave}L_b/D_b=(\ell_p^a f_b^{max} + \ell_r f_b^{res})/D_b$ , i.e., a value less than the local strength, but greater than the residual limit:  $f_b^{ave}=2.5\text{MPa} > f_b=1.3\text{MPa}$ .